AGU PUBLICATIONS

JGR

Journal of Geophysical Research: Solid Earth

RESEARCH ARTICLE
10.1002/2013JB010836

Key Point:
- A cluster of events is investigated and found to be induced

Correspondence to:
R. Schultz,
Ryan.Schultz@aer.ca

Citation:
Schultz, R., V. Stern, and Y. J. Gu (2014), An investigation of seismicity clustered near the Cordel Field, west central Alberta, and its relation to a nearby disposal well, *J. Geophys. Res. Solid Earth*, *119*, doi:10.1002/2013JB010836.

Received 19 NOV 2013
Accepted 31 MAR 2014
Accepted article online 3 APR 2014

An investigation of seismicity clustered near the Cordel Field, west central Alberta, and its relation to a nearby disposal well

Ryan Schultz[1], Virginia Stern[1], and Yu Jeffrey Gu[2]

[1]Alberta Geological Survey, Edmonton, Alberta, Canada, [2]Department of Physics, University of Alberta, Edmonton, Alberta, Canada

Abstract Historically, seismicity documented in the Western Canada Sedimentary Basin has been relatively quiescent and earthquakes are usually restricted to the foreland belt of the Rocky Mountains. However, exceptional clusters of events, which have remained active for decades, are recognized in Alberta. In this study we investigate the seismicity in this region using data obtained from recently established regional arrays, emphasizing the relationship between a disposal well in the Cordel Field and a nearby cluster of previously reported earthquakes. We explore temporal correlations of wastewater pumping rates and local seismic activity dating back to 1960. We find that the first statistically significant increase in seismicity lags the onset of wastewater injection (October 1991) by ~3.33 years. In particular, the waveform similarity of 32 events are analyzed from continuous data recorded at NOR, a nearby (~30 km) station operated by the University of Alberta starting in September of 2006. Results from this analysis suggest that many events are well correlated in the characteristics of the waveforms and thus are likely to share a similar origin and source mechanism. The most prolific of these multiplets repeats more than 10 times sporadically throughout the entire duration of recorded data from October 2006 to March 2012. Despite the limited availability of nearby stations, which adversely affects the resolution of our analysis, hypocenter depths could be relatively accurately determined from waveform synthesis and double difference methods. The results of our analysis provide first-order evidence that the seismicity is consistent with fluid injection-induced events.

1. Introduction

Fluid injection or extraction from reservoirs are known to alter the stress conditions in rocks and, in the presence of existing faults, may lead to increased seismic hazard [*McGarr et al*., 2002]. Many instances have been documented in recent years where seismic activity was linked to fluid injection [*Hsieh and Bredehoeft*, 1981; *Healy et al*., 1968; *Ahmad and Smith*, 1988; *Cox*, 1991; *Ake et al*., 2005]. The disposal of waste fluid at injection wells has well-documented cases of induced seismicity [*Healy et al*., 1968; *Raleigh et al*., 1976; *Ake et al*., 2005]. Recent earthquakes near Dallas and Fort Worth, Texas [*Frohlich*, 2012], and Guy, Arkansas [*Horton*, 2012], presented compelling case studies of disposal-related seismicity. In the latter region, disposal wells in the Fayetteville Shale field have been shut down in response to the earthquake swarm in 2010. Induced seismicity from injection wells are typically identified through a set of criteria [*Davis and Frohlich*, 1993], such as temporal and spatial correlations, exemplified by a case study of events near Youngstown, Ohio [*Kim*, 2013]. Detailed analysis of distribution and/or focal mechanisms [*Rutledge and Phillips*, 2003] and a solid understanding of background seismicity may be necessary in more complex cases such as one in Wilzetta oilfields, Oklahoma [*Keranen et al*., 2013], where a prominent earthquake sequence occurred decades after the initiation of injection. More recently, accumulating evidence has linked the process of hydraulic fracturing to induced seismicity. Two recent examples are earthquake clusters near hydraulic fracturing operations at Eola-Robberson field in Oklahoma [*Holland*, 2011, 2013] and Horn River Basin, British Columbia [*BC Oil and Gas Commission*, 2012]. Significant public scrutiny has been placed on geothermal projects and the seismicity induced during stimulation procedures [e.g., *Deichmann and Giardini*, 2009]. For instance, at The Geysers geothermal area in northern California, a direct correlation was reported between *b* value from a power distribution and fractal dimensions of earthquake hypocenters [*Eberhart-Phillips and Oppenheimer*, 1986]. Nondouble-couple mechanisms further suggested that continued fluid injection was responsible for a statistically significant spike in the temporal variations of seismicity surrounding the geothermal area [*Ross et al*., 1996, 1999].

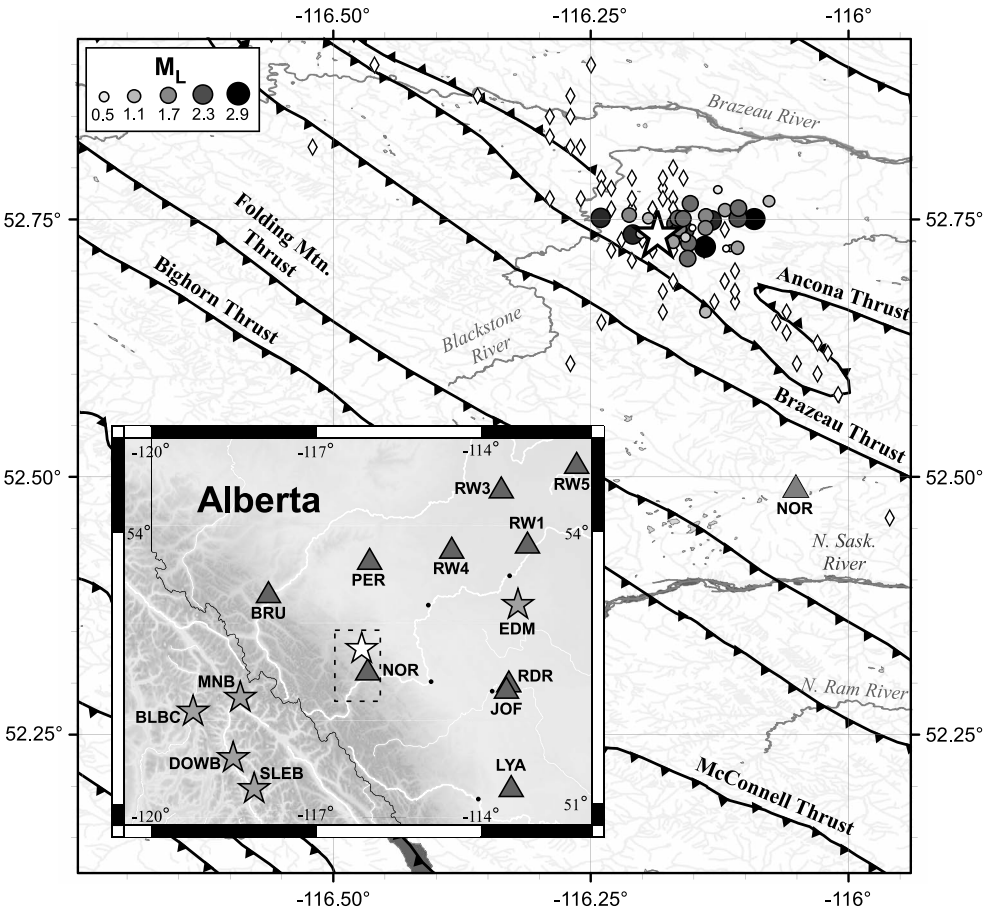

Figure 1. Spatial distribution of earthquakes from the GSC catalog (diamonds) and relocated events (circles) nearby a disposal well (white star). Locations of known faults [*Hamilton et al*., 2012] have been superimposed for reference. The embedded regional map depicts the locations of relevant CRANE (triangles) and CNSN (grey stars) stations. The dashed box indicates the local study area in relation to regional stations. Elements of this figure utilized the program Generic Mapping Tools [*Wessel and Smith*, 1998].

The targeted region in this study is in west central Alberta in the Western Canada Sedimentary Basin (WCSB). Baseline seismicity in this region is sparsely distributed, occurring chiefly along the foreland belt of the Rocky Mountains [e.g., *Stern et al*., 2013a]. Within the WCSB, an exceptional cluster of events near Rocky Mountain House has been associated with gas extraction [*Wetmiller*, 1986] due to modeled stress change below the Strachan reservoir [*Baranova et al*., 1999]. Since 1995, the rate of seismicity at the Strachan Field has significantly declined [*Stern et al*., 2013a], likely in correlation with the diminishing production from this reservoir. Second to the Strachan cluster, the Brazeau cluster (BrC), near the Cordel Field, has been one of the most consistently active regions of seismic activity in the Albertan WCSB (Figure 1). More than 10 earthquakes larger than local magnitude 3.0 have been recorded at the BrC since the mid-1990s, with events as large as 4.0 [*Earthquakes Canada*, 2012]. Despite this, no systematic spatial and temporal analysis of the seismicity in this region has been conducted to date.

In this study we utilize catalogs of events and over 4 years of continuous waveform data from the Canadian Rockies and Alberta Network (CRANE) [see *Gu et al*., 2011] and the Canadian National Seismic Network (CNSN) to examine the details of earthquakes generated at the BrC. Our analysis combines earthquake catalog data from the Geological Survey of Canada (GSC) and the Alberta Geological Survey/Alberta Energy Regulator (AGS/AER) to explore the temporal correlation of events at the BrC and to determine their relevance to disposal activities. Second, we examine the multiple character of waveforms generated at the BrC and use bootstrapped double-difference methods to increase the resolution of event hypocenters. Finally, we discuss

the relation of these events to a nearby disposal well and find that it is likely that BrC events were induced by injection activities.

2. The Cordel Disposal Well

The Cordel disposal well (CDW) is situated in the western edge of the WCSB, in the Cordel Field ~100 km northeast of the Alberta-British Columbia border. The CDW is a class II disposal well still in use for the disposal of wastewater, having injected more than 10^6 m^3 (as of December 2012) since the start of operation in October 1991. The CDW perforation interval occurs from 3796 to 3896 m depth targeting the upper Rundle Group, a middle to late Mississippian unit composed largely of limestone within its four constituent formations of Turner Valley, Elkton, Shunda, and Pekisko. The upper three formations (Turner Valley, Elkton, and Shunda) contain components of dolomite, while anhydrite is present in the Shunda [*Mossop and Shetsen*, 1994]. The overlying Fernie Formation's Poker Chip Shale and several underlying shales act as potential confining layers.

2.1. Velocity Models

The orogenesis associated with the Cordilleran deformation front results in the complex, faulted geology in the central Alberta Foothills [*Pana and Elgr*, 2013]. To accurately describe the structure of this region, we employ multiple velocity models from various sources. In all models, the sedimentary structure was determined from sonic log data at a local well and assuming a Poisson solid. In this study, Phanerozoic sedimentary layers are separated into two distinct lithologies: the lower package dates from Cambrian to Jurassic and is mostly comprised of carbonates, shales, and sandstones, while the overlying strata are clastic foreland basin deposits of mid-Jurassic to Paleocene age [*Mossop and Shetsen*, 1994]. Well log data near the CDW describe the thickness of these clastic and carbonate layers to be 3.48 and 1.64 km, respectively. The underlying crystalline basement models are more varied, although the overall crustal thickness remained static at 51 km [e.g., *Gu et al*., 2011]. Precambrian models are based on data from CRUST2.0 [*Bassin et al*., 2000] and the results from a joint inversion of teleseismic receiver function *P* phase data at the station NOR (Y. Chen et al., Crustal imprints of Precambrian orogenesis in western Laurentia, submitted to *Earth and Planetary Science Letters*, 2014). Final velocity models are compositions of the aforementioned sedimentary model and three unique basement models.

3. Correlations Between Cataloged Events and Disposal Activities

Since 1960, more than 100 earthquakes have been cataloged at the BrC by the GSC [*Halchuk*, 2009; *Earthquakes Canada*, 2012] and the AGS [*Stern et al*., 2013b], the largest two events (M_L 4.0) occurred on 31 March 1997 and 2 July 2001. Overall, the most prominent feature of seismicity at the BrC is the temporal skew of events (Figure 2a). The vast majority of large events occurred in the past 20 years, with limited relation to relevant network changes. For example, only a handful of earthquakes (less than 10, M_L 1.9–3.0) were recorded before 1990, followed by a swarm of four events (M_L 2.2–3.5) during November of 1994 despite no increase in nearby receiver density. The superposition of monthly disposal well injection volumes at the BrC reveals a possible relationship between seismic activity and injection operations. However, continual changes and improvements to the seismic network in and around the WCSB affect the detection threshold of cataloged events. For example, we observe the detection of small magnitude events ($<M_L$ 1.5) after the inclusion of nearby CRANE stations during September of 2006 (Figure 2b). To limit the impact of biases due to network setup [e.g., *Grob and van der Baan*, 2013], we truncate the composite catalogs based on the estimated magnitude of completeness. In this study, we define the magnitude of completeness as the cut-off magnitude that maximizes the goodness of fit [e.g., *Wiemer and Wyss*, 2000] to the Gutenberg-Richter frequency-magnitude relationship [*Ishimoto and Iida*, 1939; *Gutenberg and Richter*, 1942]. Based on this approach, the maximum likelihood value of seismic *b* value [*Aki*, 1965; *Marzocchi and Sandri*, 2003] and its uncertainty [*Shi and Bolt*, 1982] was estimated to be 0.999 ± 0.139 with a catalog truncation at M_L 2.24.

3.1. Seismic Rate Changes and Correlation to Injection Activities

To assess temporal patterns at the BrC, we employ ZMAP [*Wiemer*, 2001] to determine the statistical significance of changes in the rate of seismicity using β values [*Matthews and Reasenberg*, 1988; *Reasenberg and Simpson*, 1992]. This analysis of the time series data (Figure 2c) indicates that the first statistically significant increase in the rate of seismicity at the BrC occurred late in 1994, the same year that one of the

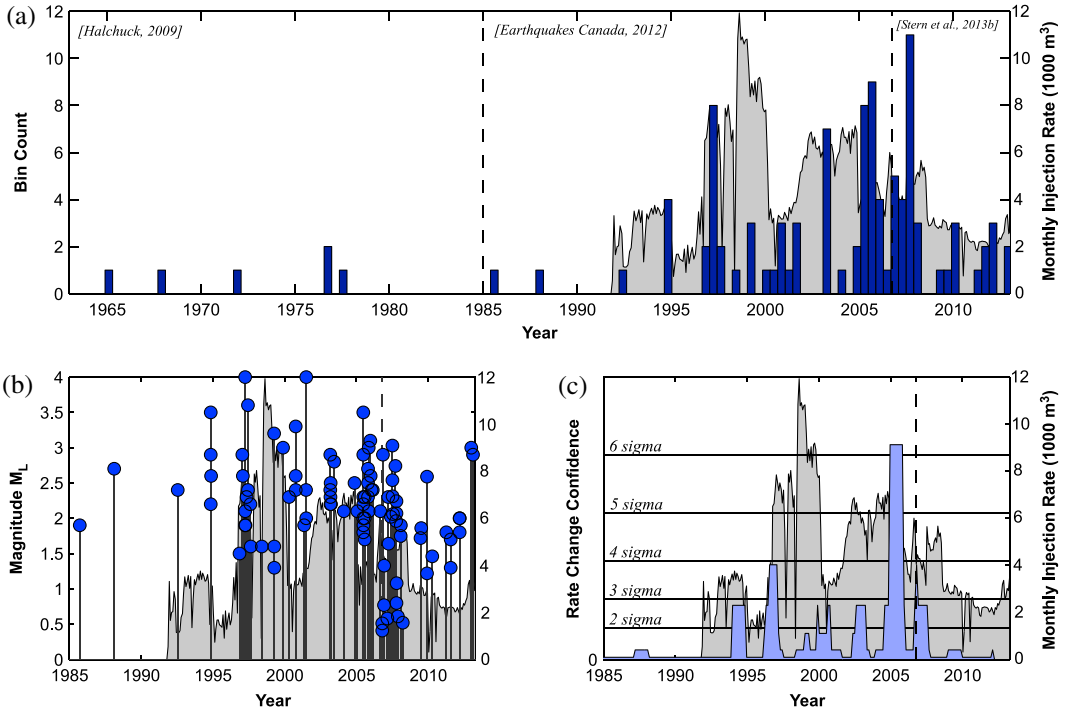

Figure 2. (a) Histogram of cataloged seismicity (blue bars) local to the BrC alongside monthly injection rates (grey curve) at the CDW. Division in catalog sources are referenced in the figure by dashed lines. (b) Temporal distribution of earthquake magnitudes (blue circles); a sudden drop in recorded magnitudes is noted at the onset of CRANE stations during late 2006. (c) Statistical confidence of the change in rate of seismicity (blue curve) as compared to injection rates. Confidence intervals are denoted by horizontal lines.

largest magnitude events was recorded at the BrC. The first increase in the rate of seismicity lags the initiation of injection by ~3 years and is followed by periods of major increase in seismicity during 1997 and 2003, which lags the expedited pumping rates by approximately 6 months and 1 year, respectively. The sharpest increase in earthquake activity was detected in early 2005, which precedes an ~8 month reduction in pumping rates. This more recent series of earthquakes includes the largest magnitude event (M_L 3.5) documented in the previous 4 years, superseded by the 2 July 2001, M_L 4.0 event that overlapped with a period of diminished injection activity. Since July 2008, continued reduction of pumping volume has been characterized by both a relatively quiescent period of seismic activity and a reduction in event magnitudes.

To assert a more quantitative assessment of the correlation between seismic activity at the BrC and injection activities, we analyze the cross correlation of their standardized time series. Furthermore, a statistical test based on surrogate time series allows for the determination of a confidence curve [e.g., *Telesca*, 2010]. Ten thousand surrogates are computed from the disposal rate time series by randomly reshuffling the data, while retaining the same power spectrum as the original signal. These surrogates are then cross correlated with the catalog time series. Confidence curves are then determined directly from the computed library of surrogate cross correlations based on the range of values greater than the desired interval. Figure 3a depicts the overlap of the correlated signals and the confidence curve. The strongest temporal correlation in seismicity at the BrC and wastewater disposal has a confidence greater than 99.7% with a delayed response time of 3.33 years, similar to the initial delay observed in seismic response. A second, statistically significant correlation ($>$ 99%) is noted with response time of 1.33 years. However, no further correlations are noted at shorter periods. Observations at larger lag times (6.5+ years) are likely due to the periodicity (~5 years) observed in the disposal rate time series coupled to previously observed correlation lag times.

3.2. Seismic Moment and Seismogenic Index

Previous studies have compared total injectant volume to cumulative seismic moment as suggested by *McGarr* [1976]. However, a lack of seismic moment data limits this application to using scaling relationships

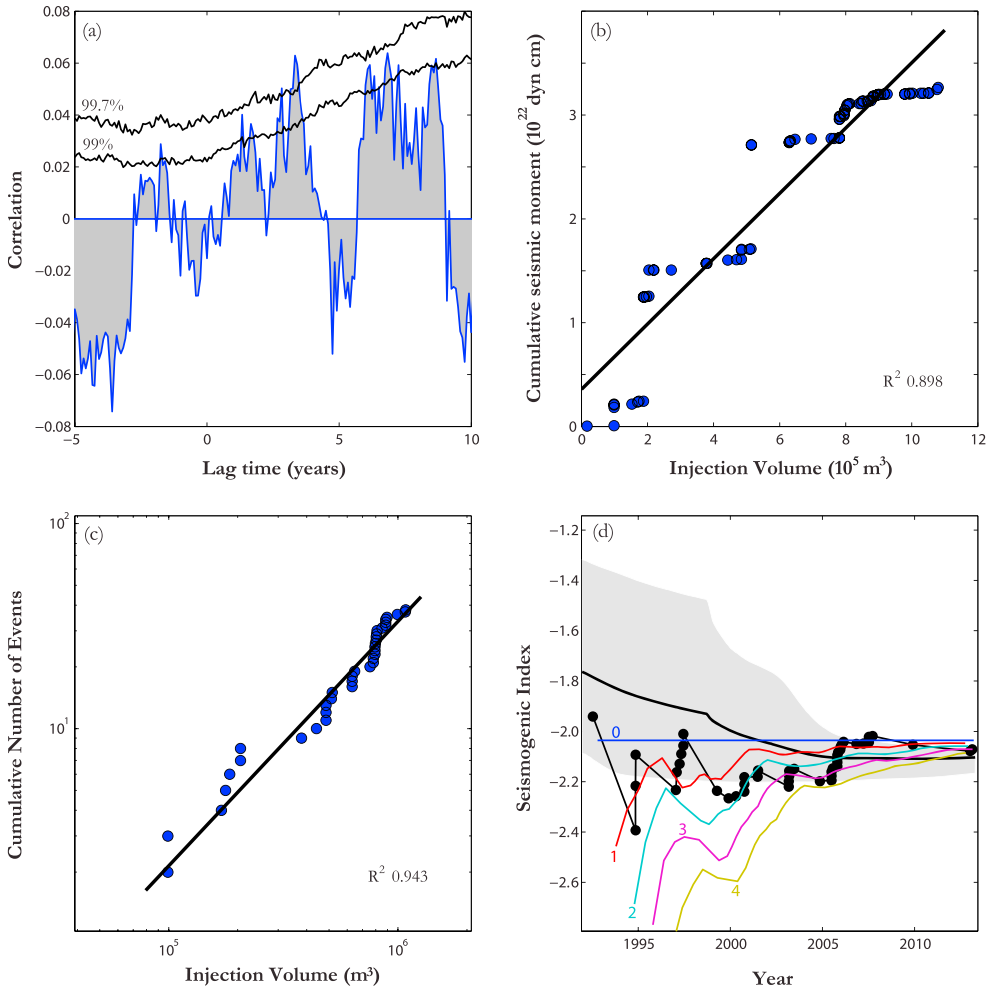

Figure 3. Correlations between wastewater disposal and seismic activity at the BrC. (a) Cross-correlation catalog time series (M_L >2.3) and of monthly disposal rates (grey filled, blue curve). Confidence intervals (black lines) are determined by reshuffling tests and labeled with their statistical significance; see text for details. (b) Scatterplot of cumulative seismic moment versus total injection volume (blue circles) and the best fit to the data (black line). (c) Log-log plot of cumulative number of events versus cumulative injection volume (blue circles) and the corresponding linear regression (black line) of the data. (d) Seismogenic index as a function of time (black circles) as calculated for the BrC. Colored lines describe seismogenic index for the idealized case where seismicity perfectly correlates with wastewater disposal, lagged by 0, 1, 2, 3, or 4 years (see contour labels). The 10th and 90th percentile in the distribution of seismogenic index values from randomly generated catalogs (grey area) and the median value (black line) are also depicted.

[*Hanks and Kanamori*, 1979] at the BrC. Despite this limitation, we still observe a linear correlation (R^2 of 0.898) between the moment and injectant quantities (Figure 3b). A linear best fit of these data is related by the apparent shear modulus [*McGarr*, 1976], estimated as 3.1 GPa N/m^2, a value on the same order as observed at the Paradox Valley disposal well [*Ake et al.*, 2005].

To further quantify the relationship between earthquake timing and injection activities, we utilize the concept of seismogenic index [*Shapiro et al.*, 2010], which characterizes the seismotectonic setting of reservoir-induced seismicity. Seismogenic index accounts for the time variability of injection-induced events by relating to cumulative volume of injectant, as a correlation has been suggested between these quantities [*Gibbs et al.*, 1973; *Shapiro et al.*, 2007]. For example, catalog time series ($M_L > 2.3$) and cumulative injection volume data from the BrC (Figure 3c) correlate well (R^2 of 0.943) throughout the entire recorded data set. In light of this relationship, *Shapiro et al.* [2010] argue based on pore pressure relaxation and a homogeneously distributed set of preexisting defects that the cumulative number of induced events N_M (t) greater than a given magnitude M is expressible as

$$\log N_M(t) = \log V_c(t) - bM + \Sigma, \quad (1)$$

where V_c (t) is the cumulative injected volume in cubic meter, b is the seismic b value, and Σ is the seismogenic index. We base our calculations on this equation and the previously determined b value ~1.0 and magnitude cutoff of 2.3 M_L. Unfortunately, the relatively small data size limits our ability to constrain the time variability of b value, hence it is necessarily assumed constant for the entire injection duration. For all cataloged events at the BrC, we observe that Σ remains relatively constant at −2.1 and varies by no more than ±0.2 after the first two recorded events (Figure 3d). We note that our value of Σ is close to the value computed (−2.5) for the Paradox Valley disposal well [*Shapiro et al*., 2010]. Lastly, the computation of Σ could be useful in future studies of seismic hazard forecasting [e.g., *Shapiro et al*., 2010; *Langenbruch et al*., 2011].

We test the validity and stability of our time dependence in Σ by comparison against synthetic catalogs. The first set of synthetic catalogs is perfectly correlated to injection activities, with a new event stimulated for approximately every 2.4×10^4 m^3 of wastewater disposed. Additionally, we incorporate time lags in seismic response to injection activities of 1, 2, 3, and 4 years (colored lines in Figure 3d) to observe the corresponding time dependence of Σ. The value of Σ remains constant for the entire injection duration, as suggested by equation (1), in the limit of instantaneous seismic response ($\log N_M(t) = \log V_c(t)$). However, we observe that a causal delay in seismic response produces a systematic bias in Σ toward more negative values. In comparison, recorded events at the BrC are largely restricted to this causal domain. We test the likelihood of this skew occurring randomly by generating 10,000 uniformly distributed catalogs and examining the resultant distribution in Σ. To ensure fair comparison, the random catalogs are restricted to the same total number of earthquakes with no events allowed to actualize before the onset of injection. Figure 3d depicts that much of the random data tends to occur at a rate faster than anticipated, especially before 2003. From this distribution, we find that the chances of randomly generating a catalog that results in a time dependent Σ with all values less than −2.0, −1.9, and −1.8 are less than 1.5, 5, and 11%, respectively.

4. Waveform Analysis and Event Multiplets

The majority of stations involved in the recording and location of BrC earthquakes are at regional distances (see Figure 1). One exception is the station NOR that has been operational since the initiation of CRANE. Using continuous data from September 2006 through 2012, we investigate the waveform signature of BrC events recorded at NOR. Furthermore, we utilize the GI Seismology Matlab Objects suite [*Reyes and West*, 2011] as a platform to examine the multiplicity of events recorded at NOR. Traces are band-pass filtered at corners of 0.8–8 Hz and aligned based on windowed cross-correlation lag times which encompass the entire waveform duration (40 s). We choose a correlation coefficient (CC) of 0.75 as the lowest allowable degree of similarity between traces to be considered event multiples.

The correlation of 32 events since September 2006 through 2012 (Figure 4) reveals that the majority of the events can be quantified as repeated earthquakes (from here on, multiplets). The most prolific series of correlated events is a tredecaplet (13 earthquakes, Figure 4b) occurring through the entire timespan (21 October 2006 to 10 March 2012) of the data (Figure 4a, cluster ID 1). Furthermore, a quintuplet (five events, Figure 4c) initiated on 28 March and took place in rapid succession on 6, 6, 8 and 17 July of 2007. The data set also contains five doublets that are separated by seemingly random intervals of time, ranging from a single day to 1.7 years. Only waveforms from four events are distinguished as unique ($CC < 0.75$) from those of other events.

We repeat the aforementioned full-waveform correlation method on the CNSN station EDM. Although EDM is much farther (~200 km) from the BrC, relevant earthquake records are available [*Earthquakes Canada*, 2013] from November 1994 to present. The analysis of these data allows us to link sparse, regionally constrained events into the multiplets of more recently located hypocenters. For example, five events during March 2003 are correlated ($CC > 0.80$) to the NOR tredecaplet earthquakes. On the other hand, data from the NOR quintuplet appears to be a small, isolated swarm of events unrelated to previous events. In addition, waveform comparisons reveal an octuplet and quintuplet of events ($CC > 0.80$ and 0.75, respectively) occurring exclusively in 2005; the octuplet is extended to 11 events based on less stringent clustering conditions ($CC > 0.70$).

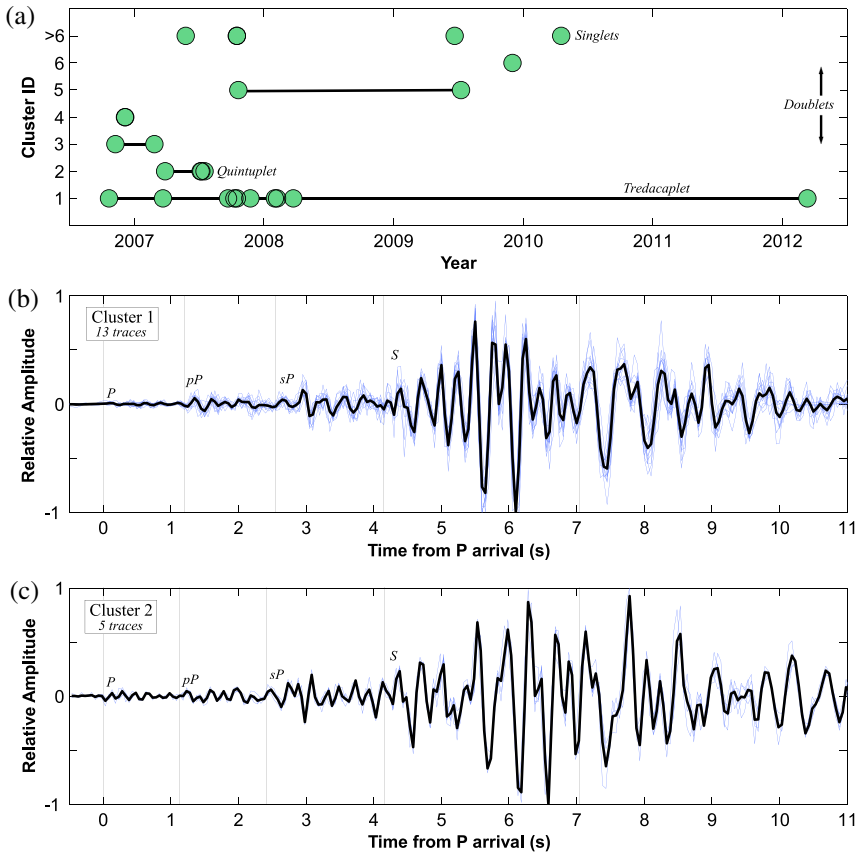

Figure 4. (a) Temporal patterns in the multiplicity of earthquake waveforms as recorded at local station NOR. Correlated earthquakes (CC > 0.75) are linked by black lines. (b) Source beam (black line) from 13 contributing (blue lines) waveforms. (c) Similarly, source beams were computed for the quintuplet. Both multiplets exhibit similar timing of crustal *P* arrivals (*pP* and *sP*) between *P* and *S* (thin black grey lines).

4.1. Extended Event Detection

Typically, event detection is either manually performed by an analyst or through an automated process, depending on the acceptable number of missed events and false alarms. Traditional detection algorithms [e.g., *Allen*, 1978] often employ short-term versus long-term averages in conjunction with nonlinear optimization of search parameters that are dependent on local geological, station, and ambient noise properties [*Vassallo et al*., 2012]. In our case, a priori information on the multiple nature of BrC events enables the application of a more powerful, multichannel cross-correlation detection algorithm [*Schaff*, 2008].

In this analysis we determine the timing of missed events through cross-correlation detection and use source beams from the local station NOR as a search template. A CC detection threshold of 0.30 is chosen to ensure a negligible probability of false alarms, a criterion in excess of the results of *Schaff* [2008]. We estimate the local magnitudes of missed events based on an empirically determined scaling relationship of maximum event amplitudes to known magnitudes. This procedure was applied to NOR data, starting at station onset in September 2006 through 2010 (Figure 5). The detection of more than 400 events, compared to 28 located events during the same time frame, is approximately consistent with the expected increase from a unit reduction in detectable magnitude [*Schaff and Waldhauser*, 2010]. The addition of small magnitude events allows us to more closely scrutinize patterns in the timing of earthquakes. For example, events at the BrC show no obvious correlation to the timing of great earthquakes [*van der Elst et al*., 2013]. Both monthly disposal rate (4500 m^3/month) and estimates of seismic moment remain roughly consistent and elevated from September 2006 to mid-2008. However, the reduction of disposal rates from 4950 to 2880 m^3/month after June 2008 is followed (~3 months later) by a notable reduction in the rate of seismicity and increase in

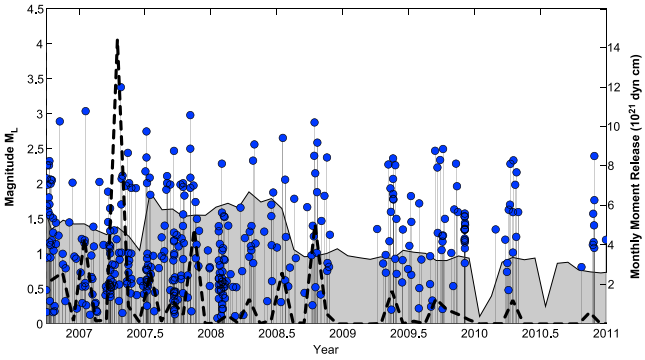

Figure 5. Temporal distribution of events, as detected by the cross-correlation detector at station NOR. Magnitudes of events (blue circles) are estimated based on an empirically determined amplitude scaling relationship. Monthly injection rates (grey curve) and moment release (thick dashed line) determined from a scaling relation are superimposed for reference. Three periods of seismic quiescence (early 2009, early 2010, and mid-2010) are noted.

monthly moment release (Figure 5). A period of total seismic quiescence ensued for approximately 4 months, ~4.5 months after the pumping rate reduction. However, this period of quiescence may be artificially extended due to a coincidental interval of elevated noise due to "sensor pops," intermittent mechanical slips in the instrument. A second period of total seismic quiescence is observed for 3.3 months, exactly coincident with a major reduction (~90%) in pumping rates on November 2009. As of mid-2008, a significant reduction in the moment release and seismicity rate has been noted, relative to prior years, and in correlation to continued reduction of disposal rates.

We repeat the same catalog-injection rate time series cross-correlation analysis (see section 3.1) as described in *Telesca* [2010] to the extended event catalog. Unfortunately, we are unable to find a statistically significant correlation between the two time series for the period of September 2006 through 2010. It is possible that the absence of statistically significant correlations at shorter periods could be attributed to the reduced/semiconstant injection rate during the study period and the low resolution (month to month) of injection data.

4.2. Waveform Constraints on Source Depth

It is well recognized that the depth variable is poorly constrained in hypocenter inversions, especially at regional distances. Often, more robust regional events constraints require local arrays with geometries on the order of the source depth [*Pavlis*, 1992; *Lienert*, 1997] or clear arrivals of regional depth phases [*Ma*, 2010; *Husebye et al*., 2013]. While the addition of CRANE stations has certainly improved the accuracy of epicentral locations (see Figure 1), the reliability of depth constraints using *P* and *S* picks are low as the closest stations NOR (~30 km) and PER (~105 km) are too far to robustly determine source depth.

In this section we exploit the richness of information in the full wavefield to provide first-order constraints on the ranges of depths applicable to events at the BrC. This is accomplished through a systematic comparison of source beams (see section 4) gathered on a common station (NOR) to synthetic seismograms computed via a reflectivity algorithm [*Herrmann and Wang*, 1985; *Gu et al*., 2005]. To mitigate the relative uncertainties and unknowns in the velocity model and moment tensor, we computed synthetics using all velocity models (and perturbed variants; see section 2.1) and several of the archetypal moment tensors. We restrict comparison to beam/synthetic envelopes to ensure that waveform comparison is concentrated on the existence, timing, and amplitude of phase arrivals rather than phase shape. Cross correlation of scaled synthetics and beam envelopes over various phase window ranges are used as our metric of waveform fit. Comparisons were subsequently performed for all velocity models and moment tensors for seismograms computed for all source depths (up to 50 km) sampled at 1 km intervals. In general, shallow waveforms contain large amplitude and later arriving surface wave energy, while deeper arrivals become increasingly sparse with gross misfit of regional depth phases between *P* and *S* arrivals. Overall, the best global fit to the waveforms is regarded as starting at 4 km depth and ending within the interval of 6–8 km (Figure 6), consistent with handpicked *pP* and *sP* arrivals compared to computed first-arrival traveltimes using TauP [*Crotwell et al*., 1999]. Amplitudes and arrival times fit quite well for all crustal *P* arrivals up to the onset of *S* waves (~4 s). However, arrivals after *S*, while still largely in phase, begin to mismatch amplitudes. It is worth noting that certain combinations of velocity model and moment tensor produce local minima in fits to the data (Figure 6, at 2 and 15 km), likely due to spurious fits of misaligned phases.

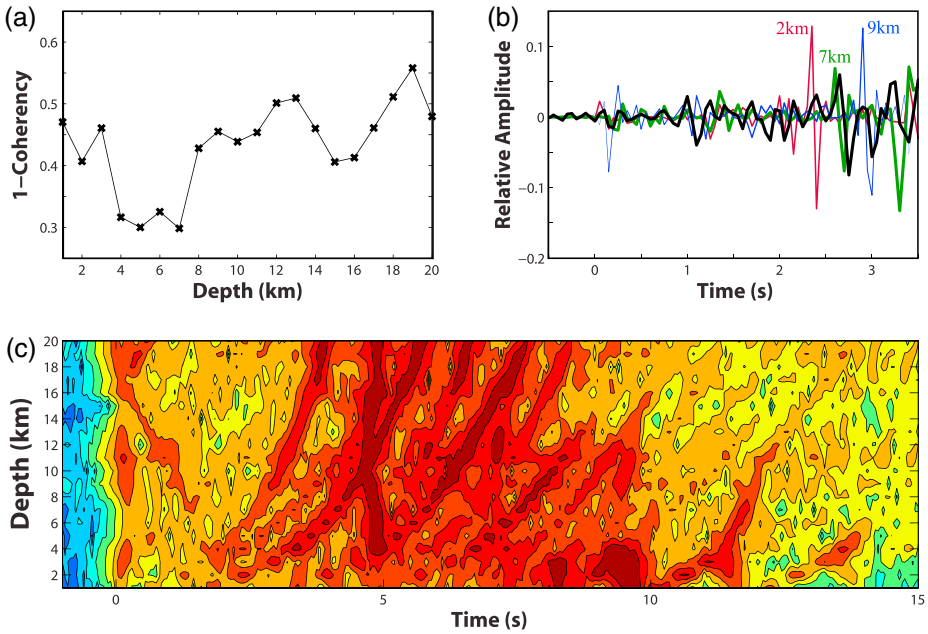

Figure 6. Source depth constraints determined for the BrC via waveform fitting of source beams; see text for details. (a) Results from waveform synthesis, windowed CCs fit to source beam for various synthetic depths, best global fit is from 4 to 7 km. (b) Sample synthetics computed for a north striking, 35° dip-slip focal mechanism at 2, 7, and 9 km source depth (labeled in panel) in comparison with the regional phases observed on the NOR beam (black line). (c) Instantaneous amplitude of the simulated wavefield, aligned on first *P* arrival.

5. Accurate Relocations of 25 Events

Waveform constraints on depth provide a first-order solution to the radial extent of BrC events and describe the distribution of earthquakes in relation to the CDW bottom. To further investigate the full, three-dimensional distribution of events, we utilize the program HypoDD [*Waldhauser and Ellsworth*, 2000; *Waldhauser*, 2001]. However, to ensure the robustness and accuracy of resultant hypocenters, we first relocate [*Pavlis et al*., 2004] cataloged events (see Figure 1) using an updated velocity model (see section 2.1) while fixing depth at a reasonably assumed value of 5 km. Hypocenter inversions are restricted to events recorded on CRANE stations [*Gu et al*., 2011] after their deployment (September 2006). From this data set of 25 events, more than 170 *P* picks and 120 *S* picks resulted in more than 1200 and 800 viable *P* and *S* differential times, respectively. Cross correlations of event pairs were determined using a windowing of 0.5 s before and 1.0 s after the phase arrival producing more than 1700 and 350 *P* and *S* waveform correlations, respectively. Double-difference relocations of epicenters limit the effects of heterogeneity and velocity model inconsistencies as well as simultaneously constraining depth [*Waldhauser and Ellsworth*, 2000]. To ensure the robustness of double-difference inversions, we resort to a bootstrap method to verify event locations; event data are decimated to 90% of its original content and then inverted. This process is iterated 1000 times for each velocity model to acquire a significant sample size and ensure consistency of the results despite relative unknowns in local structure. Final event locations and error ellipses are determined as the modal hypocenter and standard error values, respectively.

Overall, 25 event hypocenters were constrained, with mean error ellipses (2σ) of 392, 1356, and 2545 m for longitude, latitude, and depth parameters, respectively. Final RMS values for waveform cross correlations and catalog differential times are 0.309 and 0.369 ms, respectively. For all bootstrap trials the same robust features of the cluster are noted regardless of input velocity model, although the exact geometry may differ depending on the model. For example, all sedimentary events are deeper than the CDW bottom (within error) and the cluster centers are situated ~3.5 km due east, but individual hypocenters distances may be as far as 6.5 km. Departing from the robust results, one velocity model's bootstrap trial (Figure 7) details an interesting morphology of events. Extending from the uppermost sedimentary events,

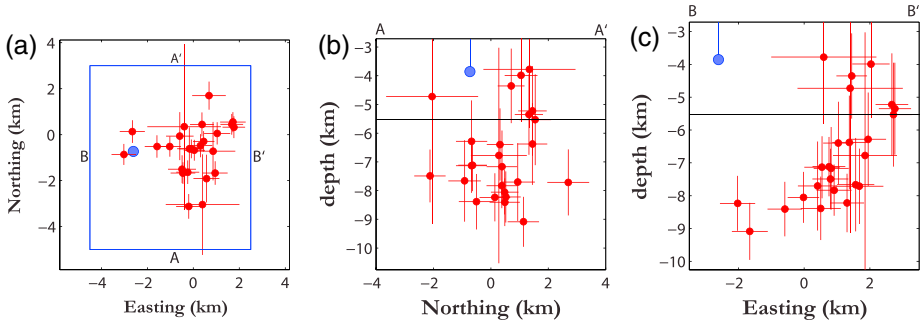

Figure 7. Robust relocations of events using bootstrapped HypoDD. (a) Epicentral scattering of events (red crosses) in proximity to the CDW (blue circle). (b) Depth cross section trending south to north shows the scatter of events, with a slight skew ~750 m north of the well bottom. (c) The depth cross section trending west to east reveals a linear trend in earthquake hypocenters. Best fit of hypocenters within the Precambrian basement (estimated by horizontal line) dip at 35° and underlie sedimentary events which are ~3.5 km directly east of the CDW bottom. (a–c) The span of event cross hairs indicates the error ellipses (0.90 confidence interval) in event relocation.

hypocenters trend along a linear feature that dips at an angle of 35° to a maximal depth of 9 km, which is well within the Precambrian basement.

6. Discussions

Tectonic earthquakes result from the rapid release of strain accumulated in the crust over geological timescales. At present, increasing research focus has been placed on understanding the acceleration of this process through human activities. In principle, the activation of an earthquake occurs when the failure condition is met: the faulting shear stress surpasses the resisting fracture stresses. Mathematically, the Mohr-Coulomb failure criteria may be expressed as [*Healy et al*., 1968]

$$\tau = \mu(\sigma_n - P) + \tau_o, \tag{2}$$

with τ representing the minimum shear stress required for nucleation, μ the coefficient of friction, σ_n the normal stress, P pore pressure, and τ_o the fault cohesion term. Two general modes of earthquake induction/triggering have been well studied from perturbations to this equation [*Simpson et al*., 1988]. The first method revolves around the modification of crustal stresses due to gravitational loading [e.g., *Pomeroy et al*., 1976] and/or poroelastic effects [*Seagall*, 1985, 1992; *Odonne et al*., 1999] involved in mass/volume flux. For a local example, poroelastic theory was applied to seismicity in the Strachan Field in the WCSB by *Baranova et al*. [1999]. Their findings suggested that seismicity below the producing formation were resultant from the modification of local stress conditions following fluid extraction. In the second method of earthquake induction, the effective normal stress is reduced through the elevation of pore pressure in existing faults [*Hubbert and Rubey*, 1959]. This process is commonly associated with the disposal of wastewater into porous strata [*Healy et al*., 1968; *Raleigh et al*., 1976; *Ake et al*., 2005] and geothermal technologies [*Majer et al*., 2007; *Deichmann and Giardini*, 2009].

In this section we argue that the features of seismicity observed at the BrC are consistent with observation of induced events. Observations of a direct correlation between the timing of injection activities and seismic activity (see section 3) is one criterion to strengthen the plausibility of a causal link [e.g., *Davis and Frohlich*, 1993]. For example, the connection to injection activity (see Figures 3b and 3c) is partially substantiated by our investigation into $\sum$, which remains relatively stable (-2.1 ± 0.2) throughout the injection history with a skew toward more negative values. This negative skew in indices can be interpreted as a causal delay in the induction of events, as evidenced by the lagged simulations (see Figure 3d). Furthermore, we observe from the generation of random catalogs that a significant portion of these events are expected to have an acausal delay and that the observed skew is statistically unlikely to be a coincidental result (see section 3.2). The delay in response between seismicity and injection activity was more rigorously determined to be 3.33 ($>$ 99.7% confidence; see Figure 3a) and 1.33 years through analysis of cross correlations and confidence curves [*Telesca*, 2010]. For induced events, delays between pumping activity and seismic response are the consequence of two features of reservoir fluid mechanics: (1) the time required for the diffusion of the pore

pressure front to a preexisting fracture network [e.g., *Seeber et al*., 2004; *Shapiro et al*., 2006] and (2) time required for the buildup of pressure to the critical Mohr-Coloumb failure threshold. This expectation is consistent with the relatively long delay (3.33 years) to the initiation of seismic activity (requiring processes 1 and 2) and potentially shorter periods (1.33 years) to seismic responses afterward. Overall, from examining cross correlations, linear regressions, and $\sum$, we find that a strong temporal correlation exists between seismic activity and wastewater injection at the BrC.

Events at the BrC share a degree of similarity (see Figure 4), which imposes constraints on the spatial separation [*Geller and Mueller*, 1980] and differences of source mechanism [*Got and Fréchet*, 1993]. In fact, the spatial separation of some of the strongest wavefield similarities ($CC > 0.90$) can be conservatively quantified [*Baisch et al*., 2008] as $\lambda/2$. In the context of the BrC, the dominant frequency of 4 Hz (at NOR) would translate to a separation interval no larger than 660 m. However, true interevent distances are likely to be closer due to the presence of noise or small perturbations in source properties. Also, the proliferation of these correlated events can be understood as the repeated relief of strain along a fault at a nucleation point of high stress [e.g., *Anooshehpoor and Brune*, 2001]. In terms of induced events, the continued elevation of pore pressure eventually reaches the critical failure condition, inducing brittle failure. This mechanism of stimulation would explain the continued repetition of multiple, nearly identical events at the BrC, assuming the continued escalation of pore pressure [*Kaiser*, 1950], analogous to geothermal stimulation studies [e.g., *Baisch and Harjes*, 2003; *Goertz-Allmann and Wiemer*, 2013]. Unfortunately, pressure data at the CDW were unavailable to scrutinize against periods of seismic activity/quiescence [e.g., *Ake et al*., 2005; *Kim*, 2013], although it is possible that a drop in pore pressure local to the fracture network resulted in the cessation of tredecaplet events (see Figure 4).

Fluid migration within fractured rock volumes tend to occur dominantly through fracture channels [*Barton et al*., 1995], which may be illuminated by earthquakes induced at critically stressed locations. Often, a prompt (hours to months) seismic response is observed nearby the injection interval after the initiation of wastewater injection. For example, at Paradox Valley, earthquakes were detected during the first weeks of injection tests, closer than a kilometer to the well bottom [*Ake et al*., 2005]. However, hydrological models have also shown that pore pressure may propagate more than 10+ km from the injection source [e.g., *Hsieh and Bredehoeft*, 1981; *Zhang et al*., 2013], potentially inducing events at similar distances from the well bottom [*Healy et al*., 1968]. At the BrC, the exact geometry of earlier events (before September 2006) is unclear due to poorer inversion constraints, although the morphology of more accurately located events (see sections 4.2 and 5) provides potential insight to the local geology at the BrC. Bootstrapped HypoDD results with various velocity models locate the BrC centroid to be ~3.5 km east from the CDW (e.g., see Figure 7). Similarly, disposal-related event clusters have been noted along lineaments as far away as ~5 km at Ashtabula, Ohio [*Seeber et al*., 2004], and ~8 km at Paradox Valley [*Ake et al*., 2005]. In particular, the delay (~5 years) noted for the initiation of events along the distant lineament (~5 km) at Ashtabula, Ohio [*Seeber et al*., 2004], is consistent with observation at the BrC (~3.5 km, 3.33 years). Furthermore, two independent methods, waveform modeling and bootstrapped HypoDD (see sections 4.2 and 5), agree that events at the BrC are largely constrained to depths at or below the injection interval. This distribution of events could suggest the presence of a preexisting fault, which would preferentially diffuse pore pressure [e.g., *Zhang et al*., 2013] into the basement, despite underlying strata. For example, results from a single velocity model's bootstrapped HypoDD show a high degree of linearity of events (see Figure 7) depicting the route of pressure migration into the basement. This result is consistent with the many cases of disposal-related seismicity that either inject into Paleozoic formations [*Raleigh et al*., 1976; *Seeber et al*., 2004; *Horton*, 2012; *Keranen et al*., 2013; *Kim*, 2013], including similarly aged Mississippian limestone [*Ake et al*., 2004], or directly into the Precambrian basement [*Healy et al*., 1968]. However, confirmation of this interpretation would greatly benefit from the addition of a tighter, local array to better constrain source geometry and focal mechanisms in view of the regional aperture of the recording array.

7. Conclusions

The WCSB is an extensive basin containing petroleum resource in North America, with more than 2500 active wastewater injection wells operating during our study period. To our knowledge, the BrC and Fort St. John cluster [*Horner et al*., 1994] are the only two cases of documented, injection-related seismicity in the WCSB.

These results seem counterintuitive, considering recent studies on the proliferation of seismicity in the central and eastern United States attributed to industry-based induction [*Ellsworth*, 2013]. In view of the results of *Goertz-Allmann and Wiemer* [2013] regarding the expected *b* values for differing crustal strength, injection intervals, and formations, it is likely that network coverage in the WCSB is too sparse to consistently detect small events. The detailed study of these "tip-of-the-iceberg" events [e.g., *Milne*, 1970] would require the extension of regional networks to accommodate larger *b* values expected for some induced events [*Shapiro and Dinske*, 2009] and the relative quiescence of the WCSB.

In conclusion, we find that the events clustered at the BrC are strongly correlated ($>$ 99.7% confidence) to the month-to-month operations at a nearby disposal well. Since the initiation of injection more than 100 events have been located at the BrC, an overall 3.5 km east bias in the centroid of BrC events from the disposal well is a persistent feature of reliably located earthquakes. This lateral bias could be interpreted as a fault structure extending into the injection formation, with the depth profile highlighting the route of hydraulic communication into the Precambrian basement. The apparent lag times between seismic activity and injection are explained as time required for the diffusion of the pore pressure front to nearly critically stressed faults and the subsequent buildup to stimulate slip. The repetition of this two-step process, pore-pressure builds to current failure criteria and then slip relieves stress coseismically, is corroborated by the high degree of event multiplicity throughout the entire waveform archive. In the past few years, a significant reduction in pumping rates appears to have reduced the recent incidence of induced seismicity at the BrC, with longer intervals in between repeated events noted. Overall, the seismicity observed at the BrC is consistent with phenomenology associated with fluid injection-induced earthquakes and is the most plausible explanation for the genesis of these events. The addition of a tighter local array would enhance efforts to understand the process of fluid induced earthquakes at the CDW. Information regarding moment tensors, source parameters, and more robust single-event location could further better examine the characteristics of quakes generated, the targeted reservoir, geomechanics of induction, and local geology at the BrC.

Acknowledgments

We would like to thank Arthur McGarr and Daniel Amorese; their insightful reviews of this paper contributed significantly to its improvement. We would like to thank Yunfeng Chen, a graduate student of Yu Jeffrey Gu at the University of Alberta, for the early use of their receiver function results used to construct Precambrian velocity models. Additionally, Jessica Dongas's work as a summer student at the AER proved invaluable; her work on sonic well logs provided the sedimentary component of our velocity models.

References

Ahmad, M. U., and J. A. Smith (1988), Earthquakes, injection wells, and the Perry Nuclear Power Plant, Cleveland, Ohio, *Geology*, *16*, 739–742, doi:10.1130/0091-7613(1988).

Ake, J., K. Mahrer, D. O'Connell, and L. Block (2005), Deep injection and closely monitored induced seismicity at Paradox Valley, Colorado, *Bull. Seismol. Soc. Am.*, *95*, 664–683, doi:10.1785/0120040072.

Aki, K. (1965), Maximum likelihood estimate of b in the formula log(N) = a-bM and its confidence limits, *Bull. Earthquake Res. Inst. Univ. Tokyo*, *43*, 237–239.

Allen, R. V. (1978), Automatic earthquake recognition and timing from single traces, *Bull. Seismol. Soc. Am.*, *68*, 1521–1532.

Anooshehpoor, A., and J. N. Brune (2001), Quasi-static slip-rate shielding by locked and creeping zones as an explanation for small repeating earthquakes at Parkfield, *Bull. Seismol. Soc. Am.*, *91*, 401–403, doi:10.1785/0120000105.

Baisch, S., and H. P. Harjes (2003), A model for fluid-injection-induced seismicity at the KTB, Germany, *Geophys. J. Int.*, *152*, 160–170, doi:10.1046/j.1365-246X.2003.01837.x.

Baisch, S., L. Ceranna, and H. Harjes (2008), Earthquake cluster: What can we learn from waveform similarity?, *Bull. Seismol. Soc. Am.*, *98*, 2806–2814, doi:10.1785/0120080018.

Baranova, V., M. Azer, and S. Bell (1999), A model for induced seismicity caused by hydrocarbon production in the Western Canada Sedimentary Basin, *Can. J. Earth Sci.*, *36*, 47–64, doi:10.1139/cjes-36-1-47.

Barton, C. A., M. D. Zoback, and D. Moos (1995), Fluid flow along potentially active faults in crystalline rock, *Geology*, *23*, 683–686, doi:10.1130/0091-7613(1995)023<0683:FFAPAF>2.3.CO;2.

Bassin, C., G. Laske, and G. Masters (2000), The current limits of resolution for surface wave tomography in North America, *Eos Trans. AGU*, *81*, F897.

BC Oil and Gas Commission (2012), Investigation of observed seismicity in the Horn River Basin, 29 pp., August. [Available at http://www.bcogc.ca/document.aspx?documentID=1270>.]

Cox, R. T. (1991), Possible triggering of earthquakes by underground waste disposal in the El Dorado, Arkansas area, *Seismol. Res. Lett.*, *62*, 113–122, doi:10.1785/gssrl.62.2.113.

Crotwell, H. P., T. J. Owens, and J. Ritsema (1999), The TauP Toolkit: Flexible seismic travel-time and ray-path utilities, *Seismol. Res. Lett.*, *70*, 154–160, doi:10.1785/gssrl.70.2.154.

Davis, S. D., and C. Frohlich (1993), Did (or will) fluid injection cause earthquakes? Criteria for a rational assessment, *Seismol. Res. Lett.*, *64*, 207–224, doi:10.1785/gssrl.64.3-4.207.

Deichmann, N., and D. Giardini (2009), Earthquakes induced by the stimulation of an enhanced geothermal system below Basel (Switzerland), *Seismol. Res. Lett.*, *80*, 784–798, doi:10.1785/gssrl.80.5.784.

Earthquakes Canada (2012), GSC, Earthquake search (on-line bulletin), Nat. Res. Can., December. [Available at http://earthquakescanada.nrcan.gc.ca/stndon/NEDB-BNDS/bull-eng.php.]

Earthquakes Canada (2013), GSC, Earthquake continuous waveform archive, Nat. Res. Can., May, AutoDRM@seismo.NRCan.gc.ca.

Eberhart-Phillips, D., and D. H. Oppenheimer (1986), Induced seismicity in The Geysers Geothermal Area, California, *J. Geophys. Res.*, *91*, 11,463–11,476, doi:10.1029/JB089iB02p01191.

Ellsworth, W. L. (2013), Injection-induced earthquakes, *Science*, *341*, doi:10.1126/science.1225942.

Frohlich, C. (2012), Two-year survey comparing earthquake activity and injection-well locations in the Barnett Shale, Texas, *Proc. Natl. Acad. Sci. U.S.A.*, *109*, 13,934–13,938, doi:10.1073/pnas.1207728109.
Geller, R. J., and C. S. Mueller (1980), Four similar earthquakes in central California, *Geophys. Res. Lett.*, *7*, 821–824, doi:10.1029/GL007i010p00821.
Gibbs, J. F., J. H. Healy, C. B. Raleigh, and J. Coakley (1973), Seismicity in the Rangely, Colorado, area: 1962-1970, *Bull. Seismol. Soc. Am.*, *63*, 1557–1570.
Goertz-Allmann, B. P., and S. Wiemer (2013), Geomechanical modeling of induced seismicity source parameters and implications for seismic hazard assessment, *Geophysics*, *78*, KS25–KS39, doi:10.1190/geo2012-0102.1.
Got, J., and J. Fréchet (1993), Origins of amplitude variations in seismic doublets: Source or attenuation process?, *Geophys. J. Int.*, *114*, 325–340, doi:10.1111/j.1365-246X.1993.tb03921.
Grob, M., and M. van der Baan (2013), Statistical biases in microseismicity parameters, GeoConvention 2013: Integration, Calgary, Canada.
Gu, Y. J., S. C. Webb, A. Lerner-Lam, and J. B. Gaherty (2005), Upper mantle structure beneath the eastern Pacific Ocean ridges, *J. Geophys. Res.*, *110*, B06305, doi:10.1029/2004JB003381.
Gu, Y. J., A. Okeler, L. Shen, and S. Contenti (2011), The Canadian Rockies and Alberta Network (CRANE): New constraints on the Rockies and Western Canada Sedimentary Basin, *Seismol. Res. Lett.*, *82*, 575–588, doi:10.1785/gssrl.82.4.575.
Gutenberg, B., and C. F. Richter (1942), Earthquake magnitude, intensity, energy, and acceleration, *Bull. Seismol. Soc. Am.*, *32*, 163–191.
Halchuk, S. (2009), Seismic Hazard Earthquake Epicentre File (SHEEF) used in the fourth generation seismic hazard maps of Canada, *Geological Survey of Canada Open File 6208*, 16 pp.
Hamilton, W. N., C. W. Langenberg, M. Price, D. K. Chao (2012), Major Bedrock Faults of Alberta (GIS data, line features, shown on AGS Map 236), Energy Resources Conservation Board, ERCB/AGS Digital Data 2012-0016. [Available at http://www.ags.gov.ab.ca/publications/abstracts/DIG_2012_0016.html.]
Hanks, T. C., and H. Kanamori (1979), A moment magnitude scale, *J. Geophys. Res.*, *84*, 2348–2350, doi:10.1029/JB084iB05p02348.
Healy, J. T., W. W. Rubey, D. T. Griggs, and C. B. Raleigh (1968), The Denver earthquakes, *Science*, *161*, 1301–1310, doi:10.1126/science.161.3848.1301.
Herrmann, R. B., and C. Y. Wang (1985), A comparison of synthetic seismograms, *Bull. Seismol. Soc. Am.*, *75*, 41–56.
Holland, A. A. (2011), Examination of possibly induced seismicity from hydraulic fracturing in the Eola Field, Garvin County, Oklahoma, *Oklahoma Geological Survey Open-File Report, OF1–2011*, 31 pp.
Holland, A. A. (2013), Earthquakes triggered by hydraulic fracturing in South-Central Oklahoma, *Bull. Seismol. Soc. Am.*, *103*, 1784–1792, doi:10.1785/0120120109.
Horner, R. B., J. E. Barclay, and J. M. MacRae (1994), Earthquakes and hydrocarbon production in the Fort St. John area of northeastern British Columbia, *Can. J. Explor. Geophys.*, *30*, 39–50.
Horton, S. (2012), Disposal of hydrofracking waste fluid by injection into subsurface aquifers triggers earthquake swarm in central Arkansas with potential for damaging earthquake, *Seismol. Res. Lett.*, *83*, 250–260, doi:10.1785/gssrl.83.2.250.
Hsieh, P. A., and J. D. Bredehoeft (1981), Reservoir analysis of the Denver earthquakes: A case of induced seismicity, *J. Geophys. Res.*, *86*, 903–920, doi:10.1029/JB086iB02p00903.
Hubbert, M. K., and W. W. Rubey (1959), Role of fluid pressure in mechanics of overthrust faulting, *Geol. Soc. Am. Bull.*, *70*, 115–206, doi:10.1130/0016-7606(1959)70[115:ROFPIM]2.0.CO;2.
Husebye, E. S., T. Matveeva, and Y. V. Fedorenko (2013), Focal-depth estimation using Pn-coda phases including pP, sP, and Pmp, *Bull. Seismol. Soc. Am.*, *103*, 1771–1783, doi:10.1785/0120120015.
Ishimoto, M., and K. Iida (1939), Observations of earthquakes registered with the microseismograph constructed recently, *Bull. Earthquake Res. Inst.*, *17*, 443–478.
Kaiser, J. (1950), Untersuchungen über das Auftreten von Geräuschen beim Zugversuch, PhD thesis, Technische Hochschule München.
Keranen, K. M., H. M. Savage, G. A. Abers, and E. S. Cochran (2013), Potentially induced earthquakes in Oklahoma, U.S.A.: Links between wastewater injection and the 2011 Mw 5.7 earthquake sequence, *Geology*, *41*, 699–702, doi:10.1130/G34045.1.
Kim, W. (2013), Induced seismicity associated with fluid injection into a deep well in Youngstown, Ohio, *J. Geophys. Res. Solid Earth*, *118*, 3506–3518, doi:10.1002/jgrb.50247.
Langenbruch, C., C. Dinske, and S. A. Shapiro (2011), Inter event times of fluid induced earthquakes suggest their Poisson nature, *Geophys. Res. Lett.*, *38*, L21302, doi:10.1029/2011GL049474.
Lienert, B. R. (1997), Assessment of earthquake location accuracy and confidence region estimates using known nuclear tests, *Bull. Seismol. Soc. Am.*, *87*, 1150–1157.
Ma, S. (2010), Focal depth determination for moderate and small earthquakes by modelling regional depth phases sPg, sPmP, and sPn, *Bull. Seismol. Soc. Am.*, *100*, 1073–1088, doi:10.1785/0120090103.
Majer, E. L., R. Baria, M. Stark, S. Oates, J. Bommer, B. Smith, and H. Asanuma (2007), Induced seismicity associated with enhanced geothermal systems, *Geothermics*, *36*, 185–222.
Marzocchi, W., and L. Sandri (2003), A review and new insights on the estimation of the b-value and its uncertainty, *Ann. Geophys.*, *46*, 1271–1282.
Matthews, M. V., and P. A. Reasenberg (1988), Statistical methods for investigating quiescence and other temporal seismicity patterns, *Pure Appl. Geophys.*, *126*, 357–372, doi:10.1007/BF00879003.
McGarr, A. (1976), Seismic moments and volume changes, *J. Geophys. Res.*, *81*, 1487–1494, doi:10.1029/JB081i008p01487.
McGarr, A., D. Simpson, and L. Seeber (2002), 40 Case histories of induced and triggered seismicity, *Int. Geophys.*, *81*, 647–661, doi:10.1016/@0074-6142(02)80243-1.
Milne, W. G. (1970), The Snipe Lake, Alberta earthquake of March 8, 1970, *Can. J. Earth Sci.*, *7*, 1564–1567.
Mossop, G. D., and I. Shetsen (1994), *Geological Atlas of the Western Canadian Sedimentary Basin*, Canadian Society of Petroleum Geologists and Alberta Research Council, Calgary, Alberta.
Odonne, F., I. Menard, G. J. Massonnat, and J. P. Rolando (1999), Abnormal reverse faulting above a depleting reservior, *Geology*, *27*, 111–114, doi:10.1130/0091-7613(1999)027<0111:ARFAAD>2.3.CO;2.
Pana, D. I., and R. Elgr (2013), Geology of the Alberta Rocky Mountains and Foothills, Alberta Energy Regulator, Map 560, scale 1:500 000.
Pavlis, G. (1992), Appraising relative earthquake location errors, *Bull. Seismol. Soc. Am.*, *82*, 836–859.
Pavlis, G. L., F. Vernon, D. Harvey, and D. Quinlan (2004), The generalized earthquake-location (GENLOC) package: An earthquake-location library, *Comput. Geosci.*, *30*, 1079–1091.
Pomeroy, P. W., D. W. Simpson, and M. L. Sbar (1976), Earthquakes triggered by surface quarrying-the Wappingers Falls, New York sequence of June, 1974, *Bull. Seismol. Soc. Am.*, *66*, 685–700.

Raleigh, C. B., J. H. Healy, and J. D. Bredehoeft (1976), An experiment in earthquake control at Rangley, Colorado, *Science*, *191*, 1230–1237, doi:10.1126/science.191.4233.1230.
Reasenberg, P. A., and R. W. Simpson (1992), Response of regional seismicity to the static stress change produced by the Loam Prieta earthquake, *Science*, *255*, 1687–1690, doi:10.1126/science.255.5052.1687.
Reyes, C. G., and M. E. West (2011), The Waveform Suite: A robust platform for manipulating waveforms in MATLAB, *Seismol. Res. Lett.*, *82*, 104–110, doi:10.1785/gssrl.82.1.104.
Ross, A., G. R. Foulger, and B. R. Julian (1996), Non-double couple earthquake mechanisms at The Geysers geothermal area, California, *Geophys. Res. Lett.*, *23*, 877–880, doi:10.1029/96GL00590.
Ross, A., G. R. Foulger, and B. R. Julian (1999), Source processes of industrially-induced earthquakes at The Geysers geothermal area, California, *Geophysics*, *64*, 1877–1889, doi:10.1190/1.1444694.
Rutledge, J. T., and W. S. Phillips (2003), Hydraulic stimulation of natural fractures as revealed by induced microearthquakes, Carthage Cotton Valley gas field, east Texas, *Geophysics*, *68*, 441–452, doi:10.1190/1.1567214.
Schaff, D. P. (2008), Semiempirical statistics of correlation-detector performance, *Bull. Seismol. Soc. Am.*, *98*, 1495–1507, doi:10.1785/0120060263.
Schaff, D. P., and F. Waldhauser (2010), One magnitude unit reduction in detection threshold by cross correlation applied to Parkfield (California) and China seismicity, *Bull. Seismol. Soc. Am.*, *100*, 3224–3238, doi:10.1785/0120100042.
Seagall, P. (1985), Stress and subsidence resulting from subsurface fluid withdrawal in the epicentral region of the 1983 Coalinga earthquake, *J. Geophys. Res.*, *90*, 6801–6816, doi:10.1029/JB090iB08p06801.
Seagall, P. (1992), Induced stresses due to fluid extraction from axisymmetric reservoirs, *Pure Appl. Geophys.*, *139*, 535–560, doi:10.1007/BF00879950.
Seeber, L., J. G. Armbruster, and W. Y. Kim (2004), A fluid-injection-triggered earthquake sequence in Ashtabula, Ohio: Implications for seismogenesis in stable continental regions, *Bull. Seismol. Soc. Am.*, *94*, 76–87, doi:10.1785/0120020091.
Shapiro, S. A., and C. Dinske (2009), Scaling of seismicity induced by nonlinear fluid-rock interaction, *J. Geophys. Res.*, *114*, B09307, doi:10.1029/2008JB006145.
Shapiro, S. A., J. Kummerow, C. Dinske, G. Asch, E. Rothert, J. Erzinger, H. J. Kümpel, and R. Kind (2006), Fluid induced seismicity guided by a continental fault: Injection experiment of 2004/2005 at the German Deep Drilling Site (KTB), *Geophys. Res. Lett.*, *33*, L01309, doi:10.1029/2005GL024659.
Shapiro, S. A., C. Dinske, and J. Kummerow (2007), Probability of a given-magnitude earthquake induced by a fluid injection, *Geophys. Res. Lett.*, *34*, L22314, doi:10.1029/2007GL031615.
Shapiro, S. A., C. Dinske, C. Langenbruch, and F. Wenzel (2010), Seismogenic index and magnitude probability of earthquakes induced during reservoir fluid stimulations, *Leading Edge*, *29*, 304–309, doi:10.1190/1.3353727.
Shi, Y., and B. A. Bolt (1982), The standard error of the magnitude-frequency b value, *Bull. Seismol. Soc. Am.*, *72*, 1677–1687.
Simpson, D. W., W. S. Leith, and C. H. Scholz (1988), Two types of reservoir-induced seismicity, *Bull. Seismol. Soc. Am.*, *78*, 2025–2040.
Stern, V. H., R. J. Schultz, L. Shen, Y. J. Gu, and D. W. Eaton (2013a), Alberta earthquake catalogue, version 1.0: September 2006 through December 2010, *Alberta Geological Survey Open File Report, 2013-15*, 36 pp.
Stern, V. H., R. J. Schultz, L. Shen, Y. J. Gu, D. W. Eaton (2013b), Alberta earthquake catalogue 2006-2010 (GIS data, point features), Alberta Energy Regulator, Digital Data 2013-0017. [Available at http://www.ags.gov.ab.ca/publications/abstracts/DIG_2013_0017.html.]
Telesca, L. (2010), Analysis of the cross-correlation between seismicity and water level in the Koyna Area of India, *Bull. Seismol. Soc. Am.*, *100*, 2317–2321, doi:10.1785/0120090392.
van der Elst, N. J., H. M. Savage, K. M. Keranen, and G. A. Abers (2013), Enhanced remote earthquake triggering at fluid-injection sites in the midwestern United States, *Science*, *341*, 164–167, doi:10.1126/science.1238948.
Vassallo, M., C. Satriano, and A. Lomax (2012), Automatic picker developments and optimization: A strategy for improving the performances of automatic phase pickers, *Seismol. Res. Lett.*, *83*, 541–554, doi:10.1785/gssrl.83.3.541.
Waldhauser, F. (2001), HypoDD: A computer program to compute double-difference earthquake locations, *USGS Open File Rep.*, *01-113*, 25 pp.
Waldhauser, F., and W. L. Ellsworth (2000), A double difference earthquakes location algorithm: Method and application to the northern Hayward fault, California, *Bull. Seismol. Soc. Am.*, *90*, 1353–1368, doi:10.1785/0120000006.
Wessel, P., and W. H. F. Smith (1998), New, improved version of the Generic Mapping Tools released, *Eos Trans. AGU*, *79*, 579, doi:10.1029/98EO00426.
Wetmiller, R. J. (1986), Earthquakes near Rocky Mountain House, Alberta, and their relationship to gas production facilities, *Can. J. Earth Sci.*, *23*, 172–181, doi:10.1139/e86-020.
Wiemer, S. (2001), A software package to analyze seismicity: ZMAP, *Seismol. Res. Lett.*, *72*, 373–382, doi:10.1785/gssrl.72.3.373.
Wiemer, S., and M. Wyss (2000), Minimum magnitude of complete reporting in earthquake catalogs: Examples from Alaska, the Western United States, and Japan, *Bull. Seismol. Soc. Am.*, *90*, 859–869, doi:10.1785/0119990114.
Zhang, Y., et al. (2013), Hydrogeologic controls on induced seismicity in crystalline basement rocks due to fluid injection into basal reservoirs, *Groundwater*, *51*, 525–538, doi:10.1111/gwat.12071.